NASA Technical Memorandum 102875

Instantaneous Velocity Field Measurement of Objects in Coaxial Rotation Using Digital Image Velocimetry

Y.-C. Cho and H. Park

October 1990

National Aeronautics and Space Administration

NASA Technical Memorandum 102875

Instantaneous Velocity Field Measurement of Objects in Coaxial Rotation Using Digital Image Velocimetry

Y.-C. Cho and H. Park, Ames Research Center, Moffett Field, California

October 1990

National Aeronautics and
Space Administration

Ames Research Center
Moffett Field, California 94035-1000

Instantaneous velocity field measurement of objects in coaxial rotation using digital image velocimetry

Y.-C. Cho and H. Park*

NASA Ames Research Center, Moffett Field, CA 94035-1000

ABSTRACT

For its experimental validation, digital image velocimetry is applied to determine the instantaneous velocity field of objects rotating around an axis with a constant angular velocity.

ACRONYMS

CC	cross correlation
CPSD	cross-power spectral density
DIV	digital image velocimetry
FT	Fourier transform
LSV/PIV	laser-speckle velocimetry or particle-image velocimetry
PSD	power spectral density
SEI	single-exposure image

1. INTRODUCTION

Digital image velocimetry (DIV) is a new technique for measuring the instantaneous velocity fields of time-dependent flows or of a collection of objects moving with spatially varying velocities.[1] This technique was developed in an attempt to eliminate some serious restrictions of previously developed optical methods, such as laser-speckle or particle-image velocimetry (LSV/PIV).[2-7] The restrictions include limited dynamic range and directional ambiguity of velocity vectors.

In ref. 1, the merits of DIV were examined by using numerically generated images representing objects in uniform motion. For the present study, a video camera was used to capture images of objects rotating around an axis with a constant angular velocity. This experiment contains most attributes needed for the experimental validation of DIV. The data contain sensing noise, image distortion, randomness of object distribution, and spatial variation of velocities.

2. DIGITAL IMAGE VELOCIMETRY

DIV was discussed in depth in ref. 1. Here it will be briefly reviewed with emphasis on the aspects that distinguish it from the optical methods. Unlike in LSV/PIV, in DIV sequential, single-exposure images (SEI) are used; these are captured using video cameras or using other techniques, such as holography.[8] Note that during image detection each frame must be accurately positioned; also, the images of each frame should be free of local distortion relative to those of other frames.

The sampled images are digitized and enhanced on the image processor. They can be linearly superposed to form an image that is equivalent to a multiple-exposure image used in LSV/PIV. Nevertheless, there is a subtle but important difference

*Summer student from University of California, Berkeley, California.

between the superposed image and the multiple-exposure image. For the latter, the correlation between the images of an object deteriorates as the images overlap. This effect contributes to the lower limit of the dynamic range of the velocity measurement by LSV/PIV. For the superposed image, however, the correlation can be maintained all the time. The superposition is not necessary for the analysis of the sequential SEIs, except for the estimation of the sampling-window sizes for determining local velocities.

The second advantage of DIV is that the time history of the SEIs is available, and it can be used to determine the direction (positive or negative) of the velocity vectors.

A third advantage of DIV can be found when determining detailed motions of densely populated objects that have a similar shape, such as seed particles embedded in fluid for the study of vortices, wake fields, turbulences, etc. With a high population density, two adjacent objects are likely to cast similar images on each single exposure; LSV/PIV will then yield false velocities from such image pairs. Faults of that kind are precluded from DIV, in which the velocity is determined from the displacement of an image in one exposure from its counterpart in another exposure.

3. DATA ACQUISITION AND PROCESSING

The system under study is composed of paint spots sprayed on a plate. The plate rotates counterclockwise around an axis perpendicular to itself at the angular velocity of 30 rpm. A pair of SEIs of the rotating paint spots are captured with a video camera at the rate of 30 frames/sec. Each SEI is immediately digitized and stored on the frame buffers of a PC-based image processor. The SEIs are shown in Figs. 1a and 1b. The temporal separation of the two images is 1/30 sec. Simple as it may appear, this system is a good example of spatially varying velocities. The velocities are tangential vectors with magnitudes proportional to the radial distance of the spot from the origin of the rotation. Near the origin, velocities are small, and SEIs of a single paint spot are so close to each other that they may overlap if superposed. On the other hand, images of a spot are well separated in the far region.

For statistical analysis, it is important that the images have an even background gray level. To this end, the statistical differencing operation[9] was applied to the images in Fig. 1. Also applied were noise cleaning and threshold operations. The latter was useful for the present analysis using the Fourier transform method. The processed images are displayed in Figs. 2a and 2b.

4. SEQUENTIAL SEI ANALYSIS

For the analysis of the sequential SEIs, two statistical methods are often used: cross correlation (CC)[8,10] and Fourier transform (FT).[1] The two methods are in principle equivalent. Selection of one method over the other may be decided on the basis of the computing efficiency and the required accuracy.

Let image 1 and image 2 be represented by the gray-level functions $g1(\bar{x})$ and $g2(\bar{x})$, respectively. The CC function $R(\bar{s})$ is defined as[11]

$$R(\bar{s}) = \iint g1^*(\bar{x}) \cdot g2(\bar{x} + \bar{s}) d\bar{x} \tag{1}$$

Here the integration is carried out for the local area enclosed by the sampling window. Within each sampling area, the velocity is assumed to be uniform. The local velocity is, within a common constant factor, determined as the vector $\bar{s}$ when R is maximized.

Let G1 and G2 represent, respectively, the FT of g1 and g2 as follows:

$$G1(\bar{f}) = \iint g1(\bar{x}) \cdot \exp(-j2\pi\bar{f} \cdot \bar{x}) d\bar{x} \tag{2a}$$

$$G2(\bar{f}) = \iint g2(\bar{x}) \cdot \exp(-j2\pi\bar{f} \cdot \bar{x}) d\bar{x} \tag{2b}$$

Here the integration is again performed over the local sampling area. The superposition of the two images is represented by the linear sum p = g1 + g2. Because of the linearity of the FT, the Fourier transform P of the superposed image p is

$$P = G1 + G2 \tag{3}$$

The modulus of this function produces a fringe pattern if a faithful correlation exists between the two SEIs within the sampling area. The local velocity is then determined from the fringes. Its magnitude is inversely proportional to the fringe separation, and its orientation is perpendicular to the fringe orientation.

For the fringe pattern, one may as well use the absolute square of P, denoted by D:

$$D = |P|^2 \tag{4}$$

On inserting eqs. (2) and (3) into eq. (4), one obtains

$$D = |G1|^2 + |G2|^2 + 2\,\mathrm{Re}(G1^* \cdot G2) \tag{5}$$

The first two terms on the right side of eq. (5) represent the power spectral density (PSD) functions of images 1 and 2, respectively. Their contribution to the fringe pattern is insignificant, and the terms can be easily removed because G1 and G2 are separately available in DIV.

The last term dictates the fringe pattern. The factor in the parentheses is the cross-power spectral density (CPSD) function, denoted by S:

$$S = G1^* \cdot G2 \tag{6}$$

As can be shown readily, this CPSD function is none other than the Fourier transform of the CC function R. This confirms the earlier statement that the CC method and the FT method are equivalent.

The CPSD function is still subject to the halo effect caused by the finite size of the individual SEI, and so is the CC function. As discussed in ref. 1, the halo effect that decreases the visibility of the fringe can be eliminated by using the PSD function for an SEI. In the absence of noise, the deblurring can be achieved by applying the inverse filter $1/|G1|^2$ to the CPSD function as follows:

$$F = \mathrm{Re}(S)/|G1|^2 \tag{7}$$

Note that this function F is equivalent to the fringe function defined in ref. 1.

No real experiment can avoid noise, which may be added to the system as white background noise, sensing noise, distortion caused by the imperfection of the system, etc. In the presence of any noise, eq. (7) cannot be used for the following reason: The PSD functions have isolated zeroes. In the absence of noise, the moduli of G1 and G2 are the same, and thus the CPSD function would have zeroes at exactly the same locations as the zeroes of the PSD functions, and the fringe function in eq. (7) would behave well near the zeroes. However, with noise present, the PSD function of the second image may not have zeroes at the zeroes of the PSD function of the first image, and vice versa. Thus, the inverse filter in eq. (7) will boost the effects of noise near the zeroes of the PSD function of the first image. Consequently the filtered fringe may be so noisy as to be entirely useless.[12]

For the present study, the inverse filter is replaced by a new deblurring filter H, defined as

$$H = 1/\left(|G1|^2 + |G2|^2\right) \tag{8}$$

The corresponding fringe function is

$$\tilde{F} = H\,\mathrm{Re}(S) \tag{9}$$

This equation alleviates the difficulties associated with the zeroes of the PSD functions. Note that the filtered fringe function behaves well near a zero possessed simultaneously by G1 and G2. It can be shown that the transfer function H represents the optimum filter. A detailed discussion for this will be reported elsewhere.

The phase of the CPSD function S was used to determine the velocity direction.

5. LOCAL VELOCITIES

For the sake of discussion, processed images 1 and 2 are superposed as displayed in Fig. 3a. Determination of local velocities are described here in some detail for the four local image pairs shown with the sampling windows in Fig. 3b. Each image pair is identified with the coordinate (x,y) of its center of weight. Note that the coordinate system here is left-handed, with the origin placed at the upper left corner.

Each selected image pair differs characteristically from the others. The image pair (246,39) is a typical case in which the SEIs overlap and LSV/PIV cannot be used at all. For the image pair (197,95), the SEIs are very close to each other, and LSV/PIV may be used but with a large error. For the image pair (302,259), the SEIs are fairly well separated, and the velocity can be determined by LSV/PIV with a smaller error. The image pair (383,173) is a case of two adjacent particles casting similar images on each single exposure; LSV/PIV would yield two velocities, one of which would be incorrect.

The SEIs enclosed by each window were separately Fourier transformed by using a digital FT program other than the fast FT algorithm. The latter was found to be more time consuming for the present computation. The CPSD function is computed from the local Fourier transforms of the SEIs according to eq. (6), and the filtered fringe function was evaluated according to eq. (9).

The modulus of P, the FT of the superposed image pairs, is displayed in Figs. 4-7, part a. The fringe patterns produced by the modulus of P appear to be inadequate for the fringe measurements except for the image pair (302,259). For the image pair (246,39), the fringe pattern is badly blurred by the halo effect. For the image pair (197,95), the fringe pattern is less blurred, but the visibility is still too low to determine the fringe separation and orientation. For the image pair (383,173), the fringe pattern shows fairly good visibility, but the orientation cannot be determined unequivocally. Similar fringe patterns would be produced by LSV/PIV, except for the image pair (246,39), for which a worse fringe pattern would be produced because of the decorrelation of the image pair in the overlap.

The filtered fringe function is displayed in Figs. 4-7, part b. The fringe patterns exhibit high visibility, with the halo effects completely removed, and they will be used here to determine the velocity vectors. To this end, we consider a pair of lines AB and CD as displayed in the figures. These lines are selected as a pair of neighboring fringe valleys closest to the center. The fringe orientation is determined as the average of the slopes of these lines. The slope of each line is determined from the coordinates of a pair of points on the line, such as A and B, or C and D. The slopes of the two lines can be compared, to estimate the computation accuracy. In general, the computation is more reliable for a greater separation of the two points on the line. The fringe separation is determined easily from the coordinates of three points, two from one line (e.g., A and B) and one from the other line (e.g., C or D).

The phase of the CPSD function near the origin is displayed in Figs. 4-7, part c. The direction of the velocity vector is determined as the direction of the decreasing phase (cf eq. 10 in ref. 1). Although the phase was computed from the (unfiltered) CPSD function, its variation is stable for all the image pairs. The reason is that no zeroes of the PSD function are present near the origin, and thus the effects of noise remain minimal.

6. VELOCITY FIELD

By inspecting the superposed image shown in Fig. 3a, sampling windows were placed at 104 locations where valid local correlation appeared to exist between the two SEIs. If a sampling window were placed on a wrong area by mistake, the computed CPSD function would not exhibit a fringe pattern.

The procedure described in the last section was applied to determine the velocities at the 104 sampled locations. The velocities are displayed in Fig. 8a. The background shows the superposition of the two SEIs displayed in Figs. 1a and 1b. The velocity of each SEI pair is represented by an arrow starting from the weighted center of the pair.

In Fig. 8b, the DIV-determined velocities are compared with the velocities computed from the angular velocity and the radial distance from the origin of the rotation. The agreement is excellent. The relative difference is less than 2%. We believe that this error is not due to any deficiency of DIV, but results from the resolution limit of the images represented with the finite-sized pixels.

The relative error is found to be nearly independent of the radial distance, and it is thus inferred that DIV is efficient regardless of the ratio of the SEI separation to the individual SEI size.

The agreement between the measured and the computed velocities appears to be weaker near the origin. This discrepancy is generated by the representation error rather than by the measurement error. The representation error is inversely proportional to the number of pixels forming the line segment representing the corresponding vector.

7. CONCLUDING REMARKS

Digital image velocimetry has been successfully validated by applying it to a laboratory experiment to determine a velocity field, and its merits have been positively confirmed.

However, there still exist two drawbacks, which, we believe, can be eliminated in the near future. First, with the currently available frame rate of the video camera, the application of DIV is limited to low velocities. For example, the velocity limit is approximately 1 m/sec with the video rate of 30 frames/sec. The development of a high-speed video camera is needed for the measurement of high velocities. For example, the video rate of 10^4–10^5 frames/sec is required to determine the supersonic velocities involved in aerodynamics studies for supersonic aircraft. The technology is available and the industry is ready to build such high-speed video cameras.

An alternative solution to the low velocity limit can be provided by utilizing the holographic technique discussed in ref. 8. With this technique, the sequential images are captured on a single holographic plate by using reference beams of different incident angles for different exposures. Thus, the image of each single exposure can be retrieved later.

It should be mentioned that the high-speed movie camera is not adequate for digital image velocimetry mainly because of the frame-to-frame variation of the local film shrinkage that occurs during film development. Such shrinkage variation has been found to be large enough to generate insurmountable distortion noise.

The second drawback is associated with the use of Fourier transforms. The deblurring filter in eq. (8) helps one to determine the velocity more accurately with the Fourier transform method than with the cross-correlation method, especially when the velocity is small. However, the Fourier transform method takes more computing time than the cross-correlation method, in general. We are currently investigating whether the deblurring filter can be translated to be used with the cross-correlation method. One way to optimize the efficiency is the parallel use of the two methods, the Fourier transform method for the areas where detailed velocity determination is needed, and the cross-correlation method for the rest.

8. ACKNOWLEDGMENTS

The rotating plate with paint spray spots was provided by Dr. B. G. McLachhlan, and valuable comments by Dr. C. A. Smith were greatly appreciated.

9. REFERENCES

1. Y.-C. Cho, "Digital Image Velocimetry," *Applied Optics*, Vol. 28, pp. 740-748, 1989.

2. P. G. Simpkins and T. D. Dudderar, "Laser speckle measurement of transient Benard convection," *J. Fluid Mech.*, Vol. 89, pp. 665-671, 1978.

3. R. Meynard, "Instantaneous velocity field measurement in unsteady gas flow by speckle velocimetry," *Applied Optics*, Vol. 22, pp. 535-540, 1983.

4. C. J. D. Pickering and N. A. Halliwell, "Particle image velocimetry: improving fringe signal-to-noise ratio with a two-step photographic process," *J. Optical Soc. Am.*, Vol. A2, pp. 610-615, 1985.

5. R. J. Adrian, "Multi-point optical measurements of simultaneous vectors in unsteady flow – a review," *Int. J. Heat & Fluid Flow*, Vol. 7, pp. 127-145, 1986.

6. L. Lourenco and A. Krothapalli, "The role of photographic parameters in laser speckle or particle image displacement velocimetry," *Experiments in Fluids*, Vol. 5, pp. 29-32, 1987.

7. A. Vogeland W. Lauterborn, "Time-resolved particle image velocimetry used in the investigation of cavitation bubble dynamics," *Applied Optics*, Vol. 27, pp. 1869-1876, 1988.

8. S. Cha, J. S. Slepicka, H. Sun and Y.-C. Cho, "Application of Digital image velocimetry to displacement measurements," *Proc. Soc. Experimental Mech. International Conference on Hologram Interferometry and Speckle Metrology*, Nov. 5-8, 1990, Baltimore, Maryland.

9. W. K. Pratt, *Digital Image Processing*, John Wiley & Sons, New York, 1978, p. 323.

10. I. Kimura and T. Takamori, "Image processing of flow around a circular cylinder by using correlation technique," *Proc. the Fourth International Symposium on Flow Visualization*, ed. C. Veret, pp. 221-226, 1986.

11. J. S. Lim, *Two-Dimensional Signal and Image Processing*, Prentice Hall, New Jersey, 1990.

12. J. W. Goodman, "Coherent optical image deblurring," *Coherent Optical Engineering*, ed. F. T. Arecchi and V. Degiorgio, North-Holland Publishing Co., Amsterdam, 1976, pp. 263-280.

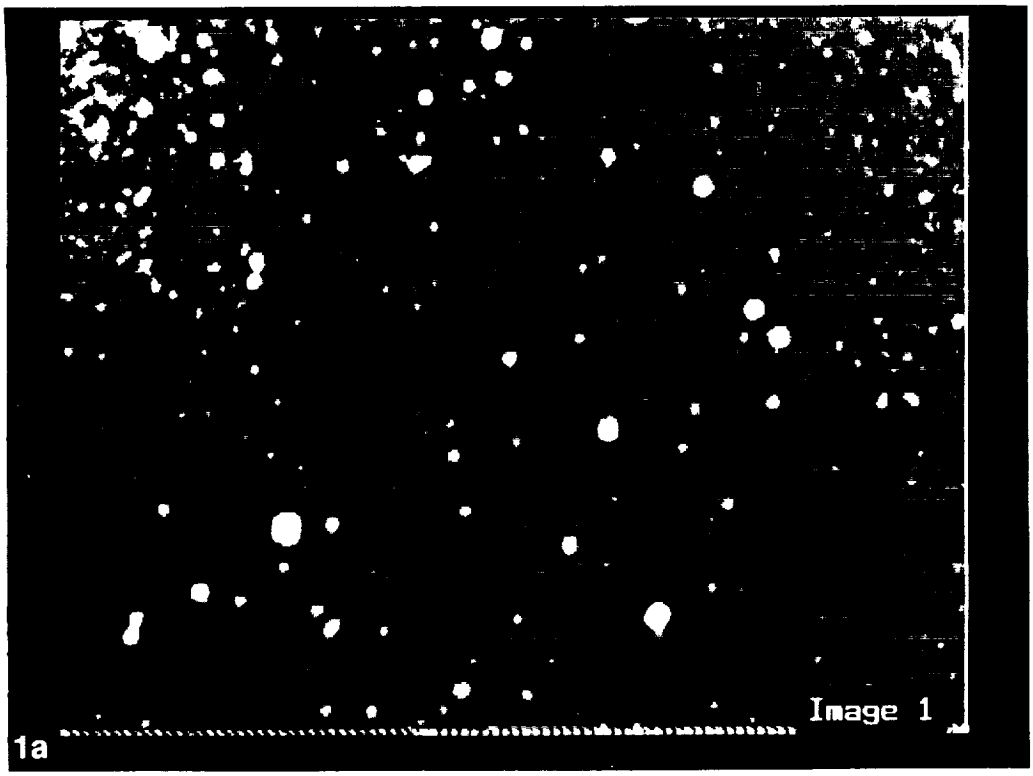

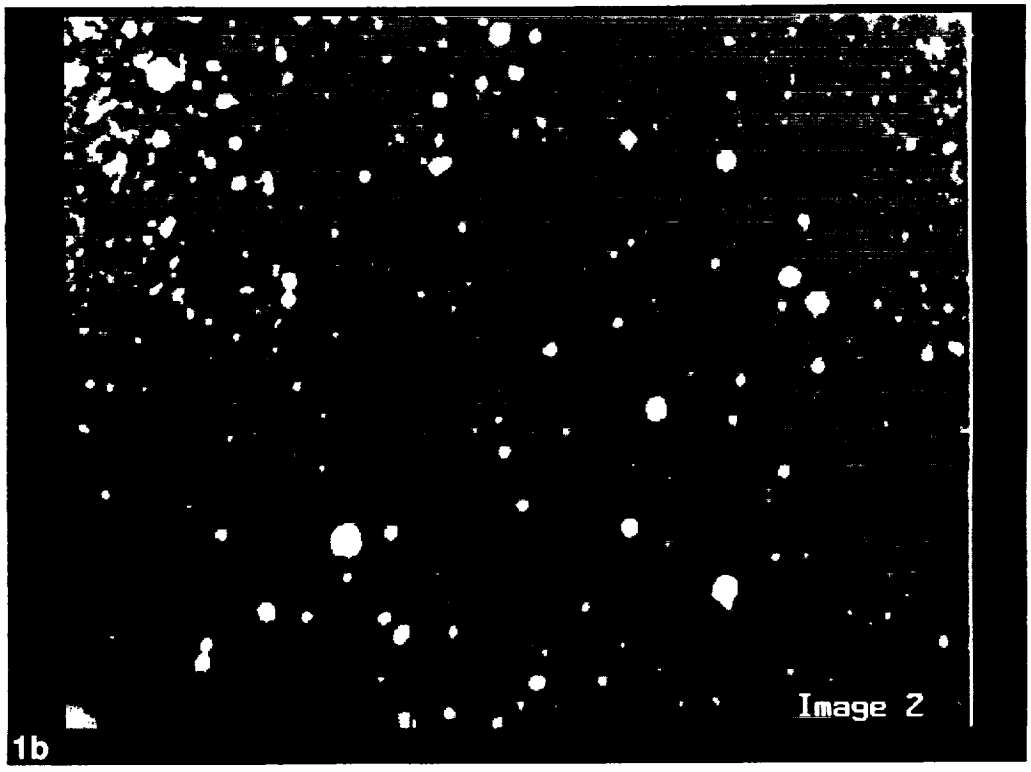

Figure 1. Two sequential single-exposure images of rotating paint spray spots; (a) image 1 and (b) image 2 are separated by 1/30 sec.

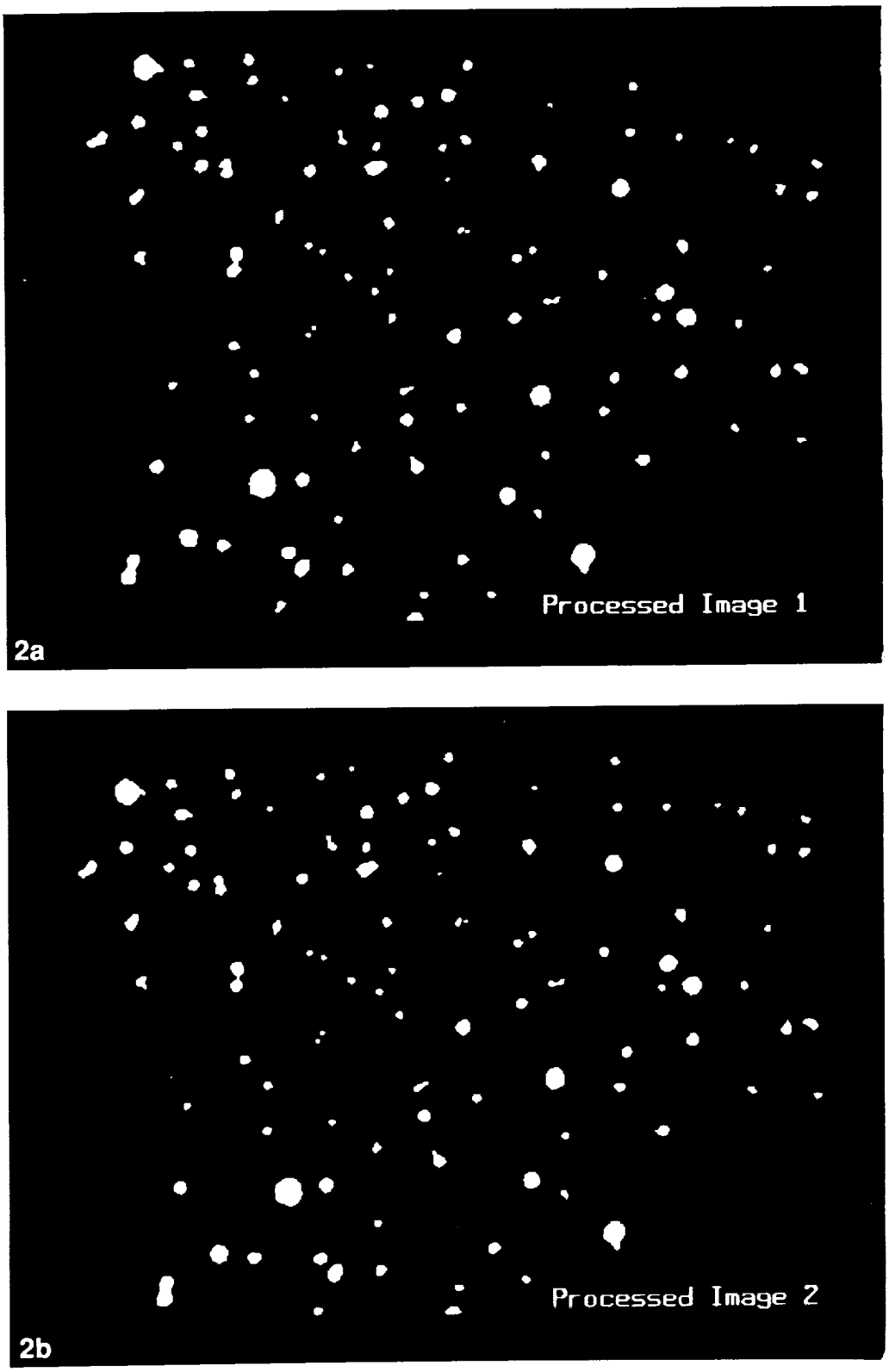

Figure 2. Digitally processed images; (a) image 1, and (b) image 2.

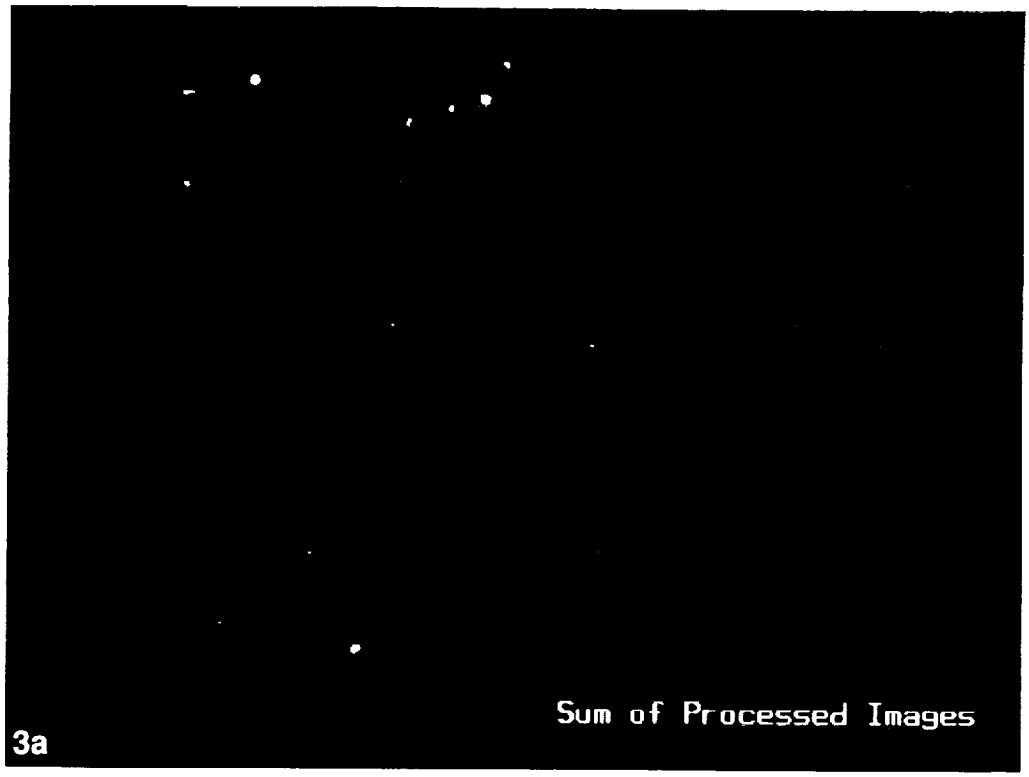

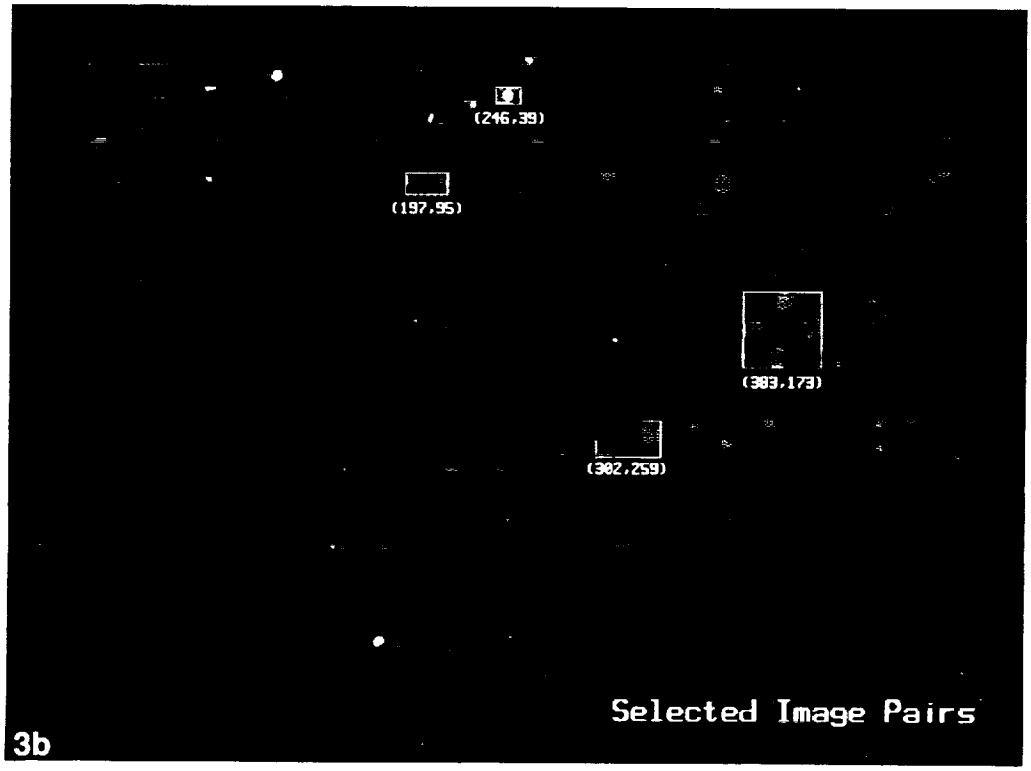

Figure 3. Linear superposition of digitally processed images 1 and 2; (a) complete superposition, and (b) superposition with sampling windows over four local image pairs identified by their coordinates.

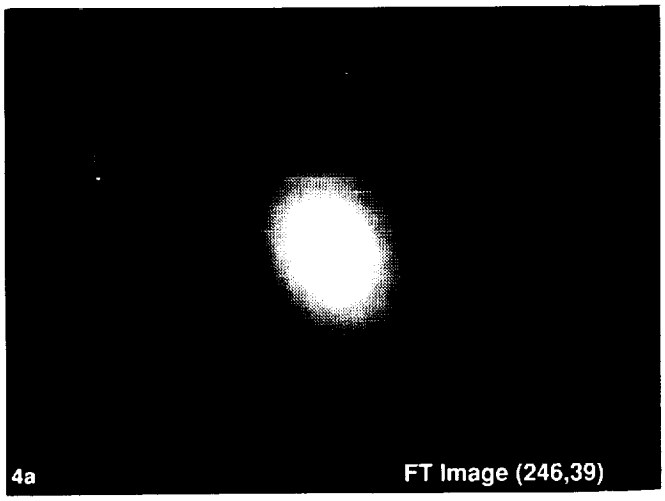

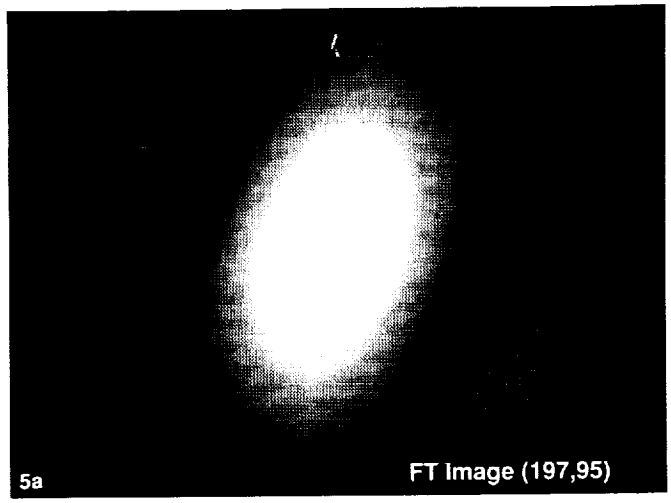

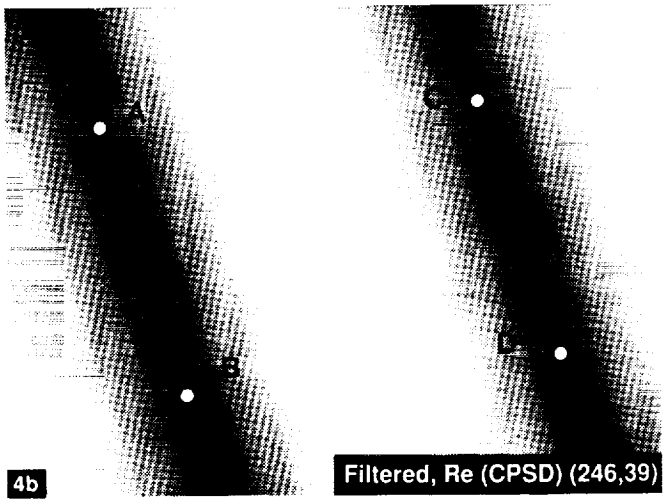

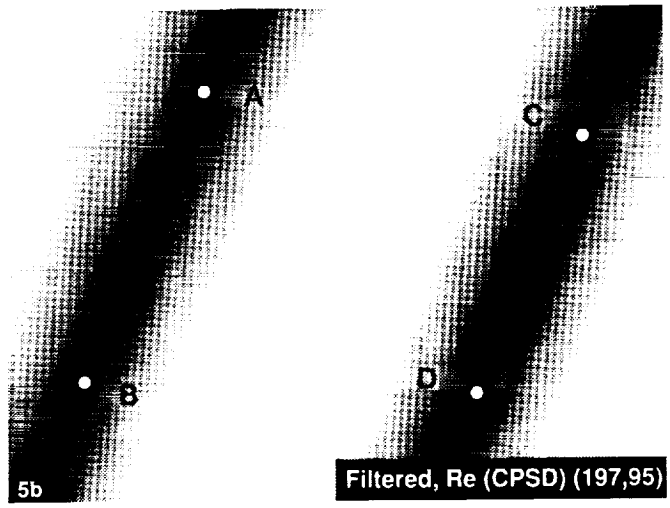

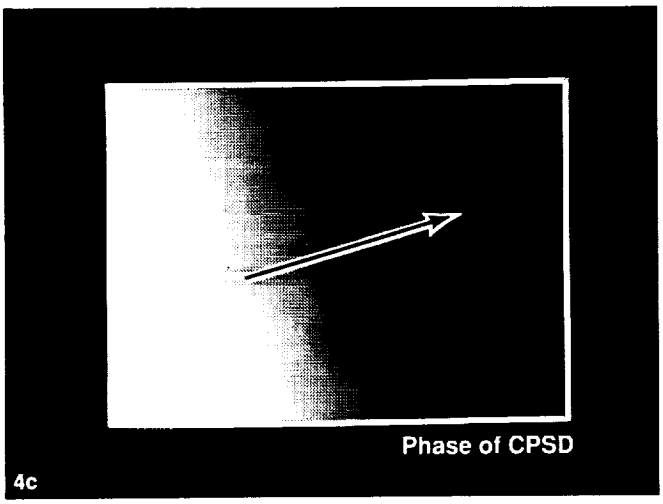

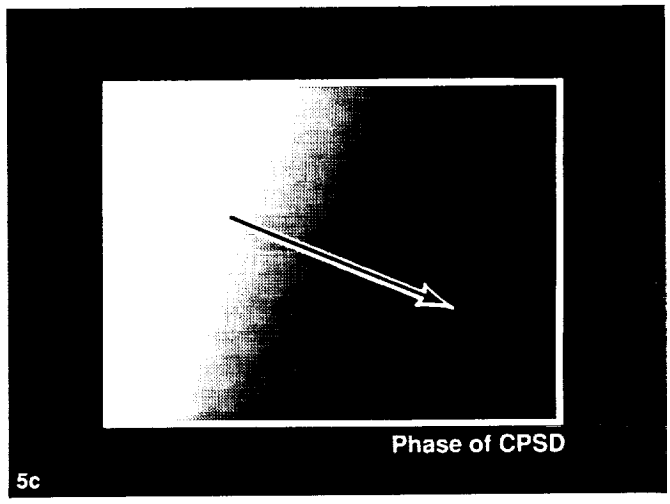

Figure 4. Fourier transform of the image pair (246,39); (a) modulus of the Fourier transform, (b) real part of the CPSD function filtered by the deblurring filter function H, and (c) phase of the CPSD function.

Figure 5. Fourier transform of the image pair (197,95); (a) modulus of the Fourier transform, (b) real part of the CPSD function filtered by the deblurring filter function H, and (c) phase of the CPSD function.

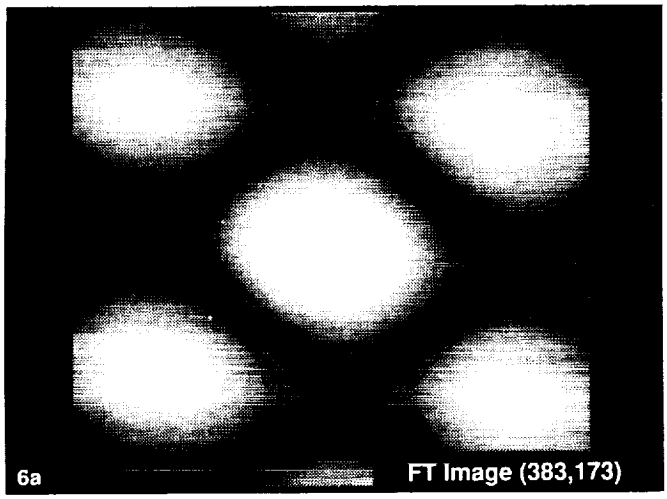

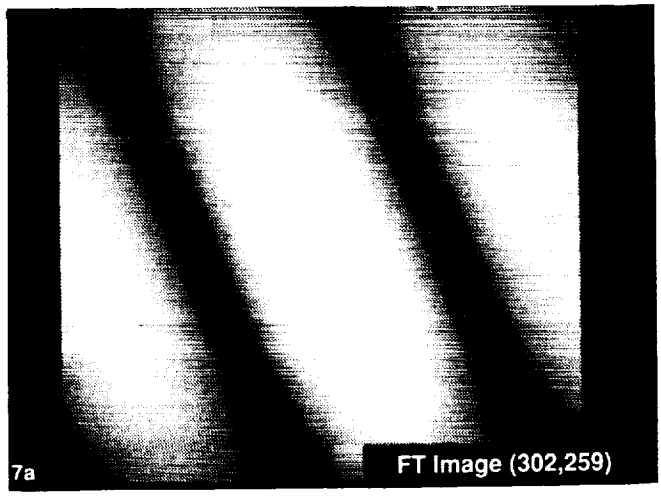

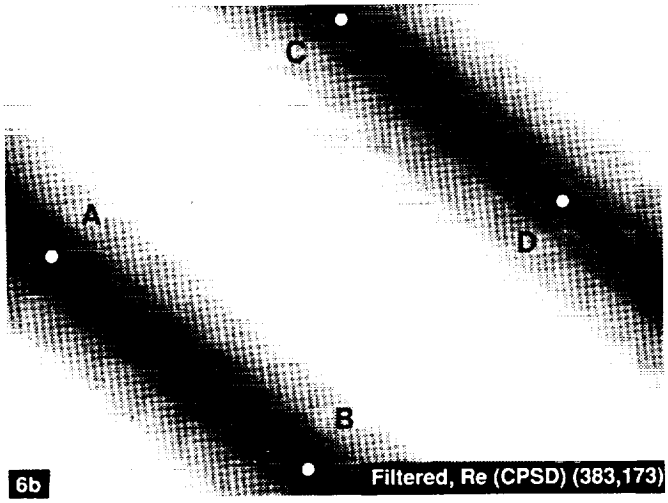

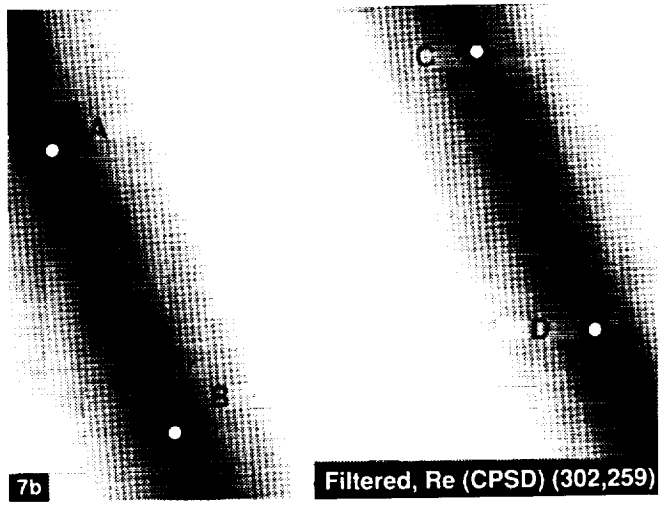

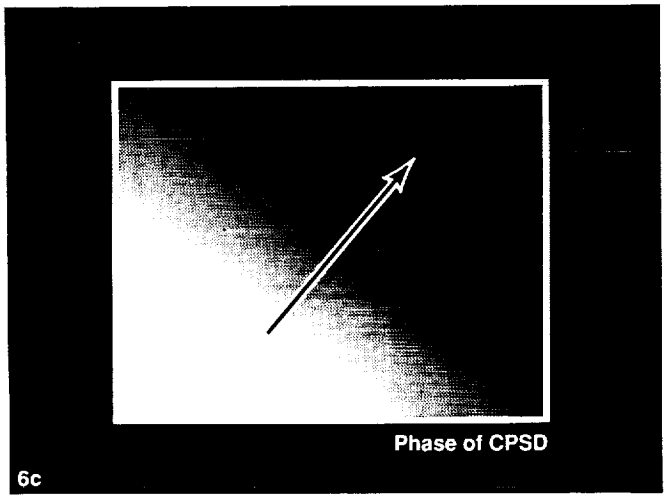

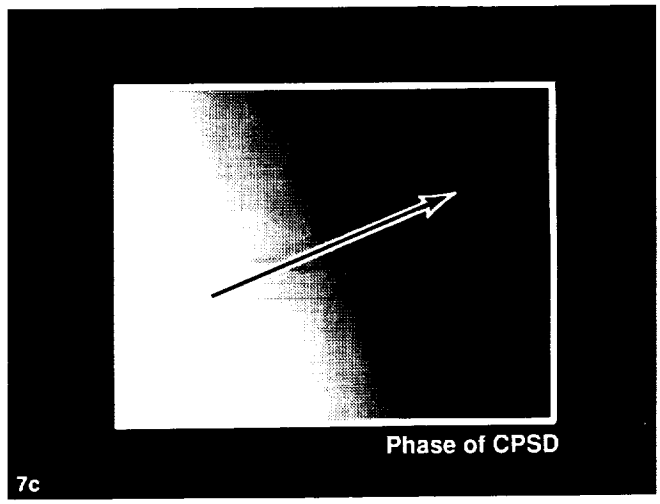

Figure 6. Fourier transform of the image pair (383,173); (a) modulus of the Fourier transform, (b) real part of the CPSD function filtered by the deblurring filter function H, and (c) phase of the CPSD function.

Figure 7. Fourier transform of the image pair (302,259); (a) modulus of the Fourier transform, (b) real part of the CPSD function filtered by the deblurring filter function H, and (c) phase of the CPSD function.

NASA
National Aeronautics and Space Administration

Report Documentation Page

1. Report No.	2. Government Accession No.	3. Recipient's Catalog No.
NASA TM-102875		

4. Title and Subtitle
Instantaneous Velocity Field Measurement of Objects in Coaxial Rotation Using Digital Image Velocimetry

5. Report Date
October 1990

6. Performing Organization Code

7. Author(s)
Y.-C. Cho and H. Park

8. Performing Organization Report No.
A-90312

10. Work Unit No.
505-61-01

9. Performing Organization Name and Address
Ames Research Center
Moffett Field, CA 94035-1000

11. Contract or Grant No.

13. Type of Report and Period Covered
Technical Memorandum

12. Sponsoring Agency Name and Address
National Aeronautics and Space Administration
Washington, DC 20546-0001

14. Sponsoring Agency Code

15. Supplementary Notes
Point of Contact: Y.-C. Cho, Ames Research Center, MS 260-1, Moffett Field, CA 94035-1000
(415) 604-4139 or FTS 464-4139
Presented at The SPIE International Symposium on Optical and Optoelectronic Applied Science and Engineering, July 8-13, 1990, San Diego, California.

16. Abstract
For its experimental validation, digital image velocimetry is applied to determine the instantaneous velocity field of objects rotating around an axis with a constant angular velocity.

17. Key Words (Suggested by Author(s))
Image processing
Velocity field measurement
Unsteady flow

18. Distribution Statement
Unclassified-Unlimited
Subject Category – 35

19. Security Classif. (of this report)	20. Security Classif. (of this page)	21. No. of Pages	22. Price
Unclassified	Unclassified	14	A02

For sale by the National Technical Information Service, Springfield, Virginia 22161

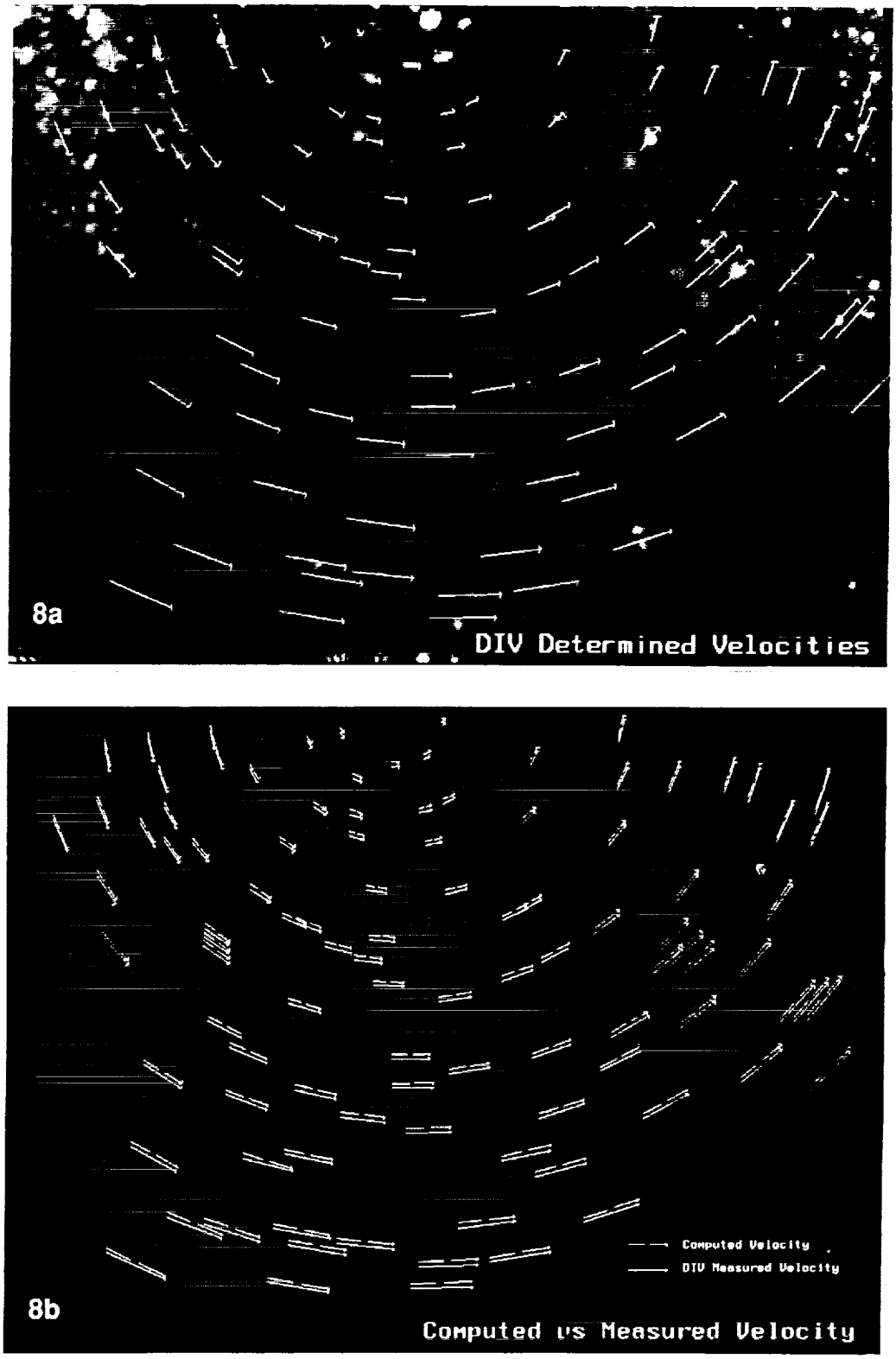

Figure 8. (a) Velocities measured by using DIV, overlaid on the superposition of raw images 1 and 2; (b) DIV-measured velocities (→), and computed velocities (— →).